Embrittlement Analysis of $\sum 5[210]/(-1-20)$ FeAl Grain Boundary in Presence of Defects: An *Ab Initio* Study

TOUKO LEHENKARI, S. ASSA ARAVINDH, WEI CAO, MATTI ALATALO, MARKO HUTTULA, and JUKKA KOMI

Iron aluminide (FeAl) inter-metallic compounds are potential candidates for structural applications at high temperatures owing to their superior corrosion resistance, high temperature oxidation, low density and inexpensive material cost. However, the presence of defects can lead to reduction in the strength and ductility of FeAl-based materials. Here we present a density functional theory (DFT) study of the effect of the presence of defects including Fe and Al vacancies as well as H dopants at the substitutional and interstitial sites at a $\sum 5[210]/(\overline{1}20)$ FeAl grain boundary focusing on the energetics. The plane wave pseudopotential code Vienna *Ab initio* Simulation Package (VASP) in the generalized gradient approximation (GGA) is used to carry out the computations. The formation energy calculations showed that intrinsic defects such as Fe and Al vacancies probably form at the GB, indicated by their negative formation energies. These vacancies can further form defect complexes with H impurities, indicated by lowered formation energies, compact bonds and charge gain of H atoms. Electronic structure analysis showed stronger hybridization of 1*s* orbitals of H with Fe and Al atoms, which leads to the stabilization of these defects resulting in degradation of material strength.

https://doi.org/10.1007/s11661-021-06450-y

I. INTRODUCTION

CORROSION-RESISTANT alloys are an essential component of industrial applications, mainly automotive, construction and novel energy conversion.[1] Currently, iron aluminides (FeAl) are drawing considerable research interest as ideal high-temperature materials to be used in high-temperature fossil fuel fired energy conversion systems, owing to the superior oxidation and sulfadization resistance.[2,3] Their many usages include but are not limited to structural materials in aircraft, heating elements and exchangers, automotive and food-handling equipment, magnetic and electronic parts, and nuclear reactor components.[3] Since the most common materials, Fe and Al, are the constituent elements of this compound, they are cheaper and have lower density compared to conventional stainless steels for structural applications. Earlier investigations on this material were mainly focused on the analysis of phase transitions as it is very important to obtain fundamental knowledge of the constituent phases.[4] These phase transitions were often accompanied by anomalous magnetic ordering owing to the associated partial disorder phenomena.[5] Apart from these advanced applications, these materials suffer from reduced low temperature ductility, and this brittleness is attributed to poor cleavage strength and/or grain boundary (GB) weakness.[6,7] Other structural defects and impurities may also co-exist with the GBs.[6,7] Hydrogen-induced embrittlement in various environmental conditions is another degradation phenomenon limiting the application of Fe alloys such as steels in general[8,9] and FeAl-based materials in particular.[10] The exposure to hydrogen can happen in two different ways in such materials. One is through the corrosion of Al, leading to the water reduction reaction due to the environmental moisture. The second option is the adsorption of hydrogen as metallic hydrogen at the surfaces, and some part of it may get released as molecular hydrogen by chemical or electro-chemical reactions. However, some hydrogen will be absorbed to the material, and this absorption will depend upon the surface coverage as well as the availability of surface sites for the hydrogen to occupy.[11] Interfaces and GBs provide such available

TOUKO LEHENKARI, WEI CAO, MATTI ALATALO, and MARKO HUTTULA are with the Nano and Molecular Systems Research Unit, University of Oulu, Penti Kaiteran Katu 1, Oulu, 90570, Finland. S. ASSA ARAVINDH is with the Nano and Molecular Systems Research Unit, University of Oulu and also with the Center for Advanced Steel Research, University of Oulu, Penti Kaiteran Katu 1, Oulu, 90570, Finland. Contact e-mail: Assa.Sasikaladevi@oulu.fi JUKKA KOMI is with the Center for Advanced Steel Research, University of Oulu.

Manuscript submitted January 5, 2021, accepted August 28, 2021.
Article published online October 9, 2021

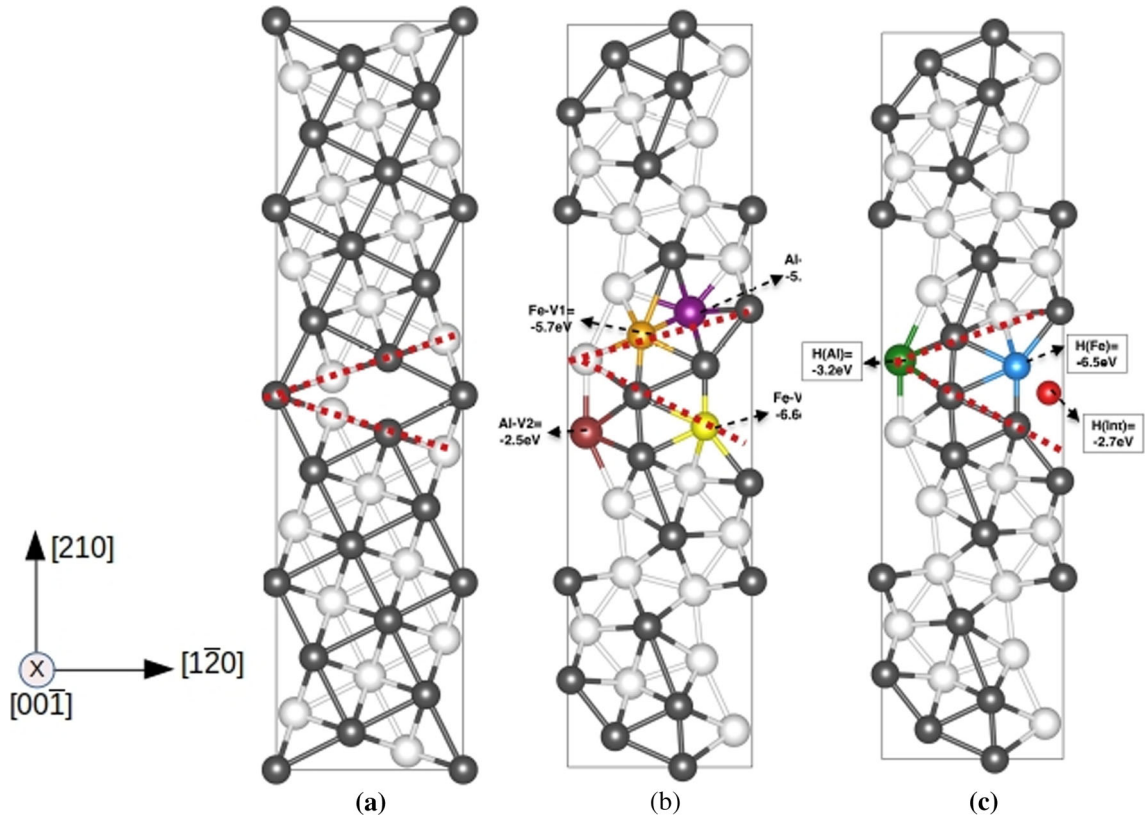

Fig. 1—(*a*) Initial and (*b*) relaxed geometry of FeAl grain boundary. (b) Fe and Al vacancy positions. The vacancy locations are indicated in different colors. (*c*) Substitutional and interstitial positions of H atom at the GB. The black and white atoms represent Fe and Al, respectively, and the red dashed lines distinguish the grain boundary region. The Visualization for Electronic and Structural Analysis (VESTA) software[28] is used to plot the figures (Color figure online).

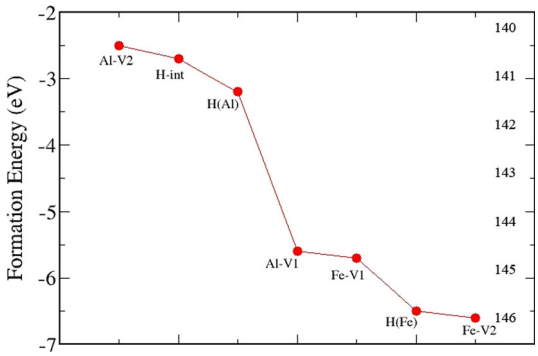

Fig. 2—Variation in formation energy (in eV) of individual defects at the FeAl grain boundary.

sites so that hydrogen can accumulate there, and extant research has shown that the presence of GBs in materials can significantly alter the properties and generate new physical phenomena.[12–15] Once hydrogen has accumulated at the FeAl GBs, it may reduce the cohesiveness of atoms leading to bond rupture and brittle fracture.[12] Attempts to enhance the ductility of the FeAl alloys have been made and include the formation of a protective oxide layer as well as introduction of ductility-enhancing elements such as Cr, B or C.[11]

Vacancies are considered the simplest type of lattice defects, and GBs are the most common planar defects. Therefore, it is crucial to understand the energetic associated with these defects and their segregation tendencies to design materials for better performance as positron annihilation and dilatometric studies have shown that different types of defects and their diffusion mechanisms determine the thermo-mechanical behavior of FeAl systems.[16] It is reported that when Fe alloys containing higher amounts of Al are exposed to atmospheric gases, these gases can react and form subsurface layers containing impurities, which is detrimental to the mechanical strength of the material.[17] Extant studies on FeAl systems are mostly oriented towards bulk systems, and investigations focusing on the collective behavior of vacancies and GBs together are needed to investigate the combined interactions of point and planar defects. The present investigation focuses on a $\sum 5[210]/(\bar{1}20)$ GB of FeAl, with the inclusion of Fe and Al vacancies. $\sum 5$ GB is selected since it is one of the most stable GBs with smaller boundary energy.[18] We investigate the energetic, magnetic and electronic properties of this material, focusing on the vacancy-induced embrittlement mechanism. Initially, the Fe and Al vacancies are placed at different locations in the GB region, and we calculated the optimized structure and corresponding vacancy formation energies. Furthermore, the H atom is introduced at the GB in substitutional and interstitial

Table I. Formation Energy of Interstitial and Substitutional H at the FeAl GB Calculated in Electron Volts (eV)

Defect Configuration	Formation Energy (eV)
$H_{int.}$ + Al–V_1	− 1.72
$H_{int.}$ + Al–V_2	− 1.22
$H_{int.}$ + Fe–V_1	− 2.78
$H_{int.}$ + Fe–V_2	− 1.62
H_{Al} + Al–V_1	− 1.08
H_{Al} + Al–V_2	− 0.11
H_{Al} + Fe–V_1	− 2.21
H_{Al} + Fe–V_2	− 1.67
H_{Fe} + Al–V_1	− 3.35
H_{Fe} + Al–V_2	− 1.77
H_{Fe} + Fe–V_1	− 3.29
H_{Fe} + Fe–V_2	− 2.38

The term H_{int} represents interstitial H. H_{Al} and H_{Fe} indicate H substituted to the Al and Fe sites. Fe–V and Al–V indicate vacancies created at the Fe and Al sites, respectively.

positions with and without intrinsic vacancies. We aim to understand the possibility of formation of intrinsic defects with and without the presence of other atomic impurities and estimate the subsequent degradation. The article is organized as follows: the computational methodology is presented in Section II, results and discussion in Section III and conclusions in Section IV.

II. METHODOLOGY

We consider the symmetric tilt boundary, $\sum 5[210]/(\overline{1}20)$, and the dimensions of the supercell are 2.87 × 25.69 × 6.42 Å^3, respectively, encompassing 20 Al and 20 Fe atoms. The GB is modeled using the aimsgb software.[19] Due to the periodic boundary conditions, the super cell contains two equivalent GBs. Nevertheless, the grains are separated by enough atomic layers so that the interactions between the GBs are negligible. The plane wave psuedopotential code Vienna *Ab initio* Simulation Package is used for the computations.[20] We employ the generalized gradient approximation (GGA) for treating the exchange and correlation.[21] The projected augmented wave-based pseudo-potentials in the Perdew Burke Eizenhoff (PAW-PBE) parameterization are used for the calculations.[22] A plane wave cut-off energy of 450 eV is used to expand the plane waves included in the basis set and a Monkhorst pack K-grid of 9 × 1 × 4 for the integration of the Brillouin zone. The GB super cell was optimized using energy and force tolerances of 10^{-06} eV and 10^{-03} eV/Å, respectively.

The formation energy (E^f) of native defects, such as Al/Fe vacancies, H in substitutional and interstitial positions as well as defect complexes were calculated using the formula[23–25]:

$$E^f(D) = \left(E_{(GB+D)} - E_{GB} \pm n_i\mu_i\right)/n_i, \qquad [1]$$

Here, the first and second terms on the right-hand side of the equation represent the total energy of the defective GB and pristine GB, respectively. The labels n_i and μ_i represent the number and chemical potential of the removed/added atoms. Chemical potentials were calculated as the total energy of the atom for the respective element.

III. RESULTS AND DISCUSSION

First, the pristine GB (the one without defects) is subjected to optimization. The starting and relaxed configurations are presented in Figures 1(a) and (b), respectively. After significant atomic relaxation, hexagonal ring-like patterns are formed at the GB, as Figure 1(b) shows.

We see that after optimization the forces on atoms at the grain boundary are minimal, and the energy convergence has been achieved within the tolerance limits. The presence of hexagonal and pentagonal rings in the supercell originates from the boundary expansion due to relaxation to reduce the lattice energy to form a stable structure, and ring patterns are formed. The resulting GB structure is stable without any dangling bonds. Such ring patterns have been reported to form in supercells containing grain boundaries.[13–15,26,27] The Fe–Al bond length in the pristine GB is 2.48 Å, and in the relaxed structure, the bonds are readjusted such that Fe-Al distances vary from 2.3 to 2.6 Å. To study the probability of formation of native defects, vacancies are created at the GB by removing one Fe/Al atom at a time such that two different vacancy positions are created for both Fe and Al. The obtained formation energies are presented in Figure 1(b) along with vacancy positions. The negative formation energies signify that the vacancies easily form at the GB. The formation energies of Fe–V_1 and Fe–V_2 are − 5.7 and − 6.6 eV while those of Al–V_1 and Al–V_2 are − 2.5 and − 5.6 eV, respectively. The lower formation energy of the Fe vacancy indicates that they are more easily formed compared to Al vacancies at the GB. The ease of formation of intrinsic defects at the GB makes it prone to other defects, such as impurity-vacancy defect complexes. Moreover, hydrogenation is one of the major degradation sources in metal surfaces and interfaces; therefore, H is introduced at the GB in both substitutional and interstitial positions. To create the substitutional positions, both Al and Fe sites are replaced with the H atom. Figure 1(c) shows the H interstitial and substitutional positions at the FeAl GB. Figure 1(c) shows that H introduced at the Fe site has a formation energy of − 6.5 eV, while at the Al site and at interstitial sites, it is − 3.2 and − 2.7 eV, respectively.

Figure 2 shows variation of formation energies for different individual defects at the FeAl GB. The lowest formation energy indicates that hydrogenation of FeAl systems can happen very easily at the interfaces and GBs leading to degradation of mechanical strength. Since H can easily stabilize at the Fe site, we further calculated the formation energies of defect complexes by introducing vacancies along with H. Various configurations were simulated such as H at the Fe site + Fe/Al vacancies, H at the Al site + Fe/Al vacancies and interstitial H + Fe/

Table II. Bader Charges of the Atoms at the GB

Configuration	Bader Charge (e)			Bond Length (Angstrom)		
	H	Fe-1nn	Al-1nn	Fe–H	Al–H	Fe–Al
H_{Al}	− 0.33	− 3.19	3	1.78	2.50	2.44
H_{Fe}	− 1.23	− 2.86	3	1.60	1.97	2.56
$H_{int.}$	− 0.33	− 1.60	3	1.73	2.27	2.39
H_{Fe} + Al–V_1	− 1.07	− 2.13	3	1.72	2.0	2.67
H_{Al} + Al–V_1	− 0.73	− 0.37	3	1.89	2.09	2.65
H_{Fe} + Fe–V_1	− 0.97	− 4.43	3	1.66	1.92	2.5
H_{Al} + Fe–V_1	− 1.04	− 2.16	3	1.71	2.17	2.51

The table shows the configurations in which H atoms are substituted to the Al/Fe site, H-interstitial and the defect complex including both H and vacancy configurations. Here, the atoms close to the H atom are considered.

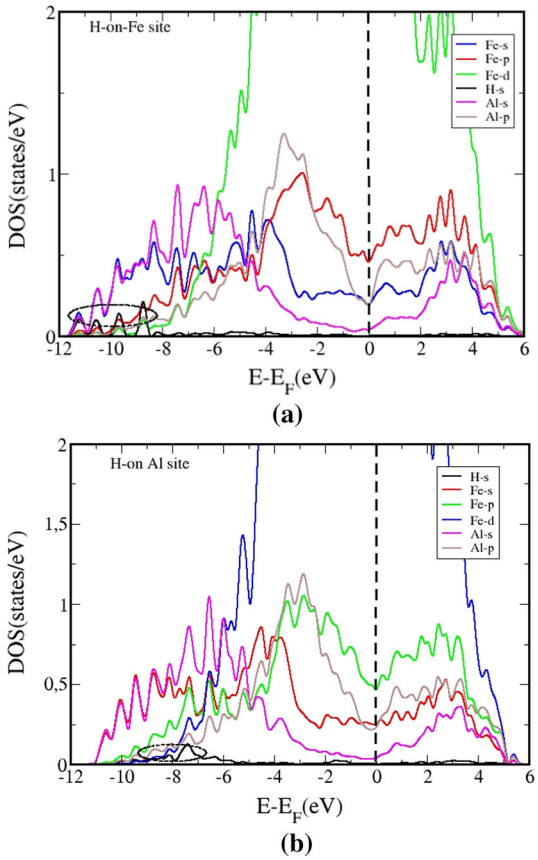

Fig. 3—(*a*) Density of states of FeAl GB with H substituted to Fe and (*b*) density of states of FeAl GB with H substituted to Al sites. The figures are plotted using the opensource software, XMGRACE.[29].

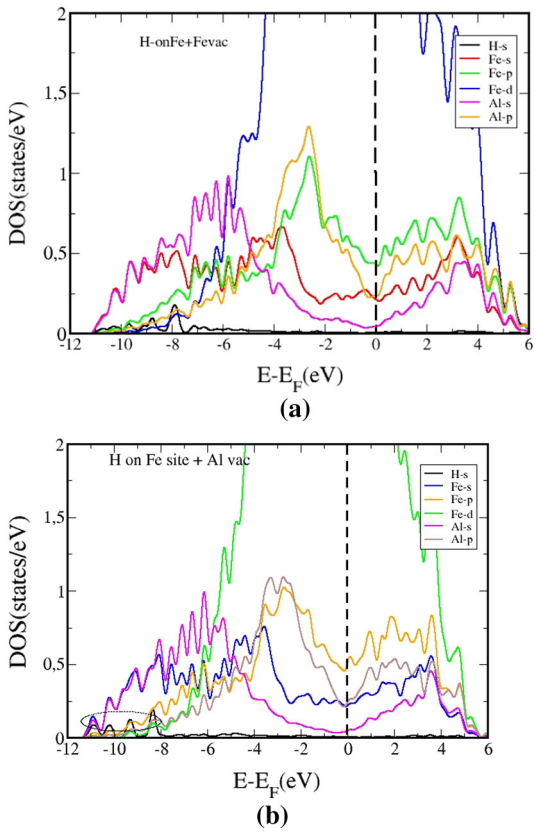

Fig. 4—(*a*) Density of states of FeAl GB with H substituted to Fe site in presence of Fe vacancy and (*b*) density of states of FeAl GB with H substituted to Fe site in presence of Al vacancy.

Al vacancies. The calculated formation energies are presented in Table I.

The lowest formation energy of − 3.35 eV is exhibited by the defect complex when H is introduced at an Fe site and an Al vacancy is present in the near vicinity. The defect configuration of H at an Fe site together with the Fe vacancy in the vicinity also shows very close formation energy of − 3.29 eV. On the other hand, H interstitial in the presence of Fe and Al vacancies requires more energy to be stabilized. To understand the formation of defect complexes in detail, we calculated the Bader charges associated with atoms, and those calculated for the atoms near the defects are presented in Table II. Since H interstitial and associated defect complexes showed higher formation energies, for further investigations we only considered the defects involving H in substitutional Fe and Al positions. The Bader charges calculated for H, Fe and Al atoms along with vacancy defects are presented in Table II. It can be seen that the H and Fe atoms gain charge, while Al atoms lose it. Interestingly, the H atom in the most stable configuration (H on Fe site) gained maximum charge (1.23 e). For the most stable defect complex, (H_{Fe} + Al-V_1), also the charge gain of H atom is higher than that of

other configurations, followed by (H_{Al} + Fe-V_1) defect complex. However, for all the nearest neighbor Al atoms, the charge reduction is uniform. For the nearest neighbor Fe atoms, the charge gain is increased for the most stable configurations. The calculated bond lengths in the near vicinity of the defects are also presented in Table II.

It can be seen that the bond lengths of H–Fe and H–Al for the most stable defect configurations are shortened, so that for H_{Fe} it is 1.60 to 1.97 Å and for H_{Fe} + Al–V_1 it is 1.72 to 2.0 Å. On the other hand, the Fe–Al bonds are elongated in these two cases to 2.56 and 2.67 Å, respectively. This indicates that more charge gain and compact bond lengths contribute to stronger bonds, leading to stable defect complexes, as evidenced by the lower formation energies.

To gain further insight into the mechanism of defect formation at the GB, we calculated the density of states (DOS) in the presence of various defect complexes as shown in Figures 3 and 4. Since formation of H interstitial requires higher energies, only substitutional He with vacancies is considered. Figure 3(a) shows the orbital and atom resolved DOS calculated for the H substituted to the Al site and Figure 3(b) shows that for H substituted at the Fe sites for the FeAl GB. The DOS shows a metallic behavior with a significant contribution at the Fermi level. The DOS contributed by Fe and Al dominates at higher energies, while 1*s* states of H appear deep inside the lower energy regions for both configurations. Figure 3(b) shows that for the H at the Al site, the contribution of 1s DOS is reduced compared to the Fe site. The presence of multiple peaks of 1*s* state of H in the GB containing H at the Fe site indicates the possibility of strong hybridization between H 1*s* states and orbitals of Al and Fe atoms. This leads to the enhanced stability of this defect. The DOS calculated for the defect complexes created by substitutional H at Fe or Al site and Fe/Al vacancies are shown in Figure 4. The strong hybridization of H with Al and Fe is shown, along with multiple peaks for the configuration with Al vacancy. These findings thus effectively support the formation energy calculations. Our results indicate that the interaction of H with native defects can thus lead to the formation of defect complexes, which are very stable and can lead to the degradation of the FeAl material.

IV. CONCLUSION

To conclude, DFT studies were conducted on the $\sum 5[210]/(\overline{1}20)$ FeAl grain boundary in the presence of native defects and H impurity. Formation energy calculations showed that both intrinsic vacancies and multiple defect complexes are prone to form at the GB. The Fe vacancies form more easily at the GB compared to Al, and H atoms prefer to substitute Fe atoms compared to Al. This can be attributed to the larger ionic radii of Al compared to Fe, which helps the defects to form easily. The interstitial H atoms require more energy to form at the GB. Occurrence of more compact bond lengths and charge sharing between atoms were noted in the vicinity of the defect, emphasizing their increased stability. Furthermore, electronic structure calculations indicated the possibility of strong hybridization of the 1*s* orbital of H impurity and Fe/Al atoms. Our studies thus reveal the importance of defects and the underlying physical mechanism that affect the stability of FeAl intermetallics for potential applications.

ACKNOWLEDGMENTS

The authors gratefully acknowledge CSC-IT, Finland, for computational resources and Academy of Finland Grant (#311934).

CONFLICT OF INTEREST

The authors declare that they have no known competing financial interests or personal relationships that could have appeared to influence the work reported in this paper.

FUNDING

Open access funding provided by University of Oulu including Oulu University Hospital.

REFERENCES

1. M. Auinger, V.G. Praig, B. Linder, and H. Danninger: *Corr. Sci.*, 2015, vol. 96, pp. 133–43.
2. P. Novák, A. Michalcová, I. Marek, M. Mudrová, K. Saksl, J. Bednarcík, P. Zikmund, and D. Vojtech: *Intermetallics*, 2013, vol. 32, pp. 127–36.
3. C.G. McKamey, J.H. De Van, P.F. Tortorelli, and V.K. Sikka: *J. Mater. Res.*, 1991, vol. 6, pp. 1779–805.
4. H. Okamoto and P.A. Beck: *Metall. Mater. Trans. B.*, 1971, vol. 2B, pp. 569–74.

5. P.R. Swann, W.R. Duff, and R.M. Fisher: *Metall. Mater. Trans. B.*, 1972, vol. 3B, pp. 413–23.
6. C.T. Liu, C.L. Fu, E.P. George, and G.S. Painter: *ISIJ Int.*, 1991, vol. 31, pp. 1192–1200.
7. C.T. Liu and E.P. George: *Scr. Metall. Mater.*, 1990, vol. 24, p. 1285.
8. A. Trautmann, G. Mori, M. Oberndorfer, S. Bauer, C. Holzer, and C. Dittmann: *Materials*, 2020, vol. 13, p. 3604.
9. F.F. Dear and G.C.G. Skinner: *Philos. Trans. R. Soc. A*, 2017, vol. 375, p. 20170032.
10. A. Barnoush, J. Dake, N. Kheradmand, and H. Vehoff: *Intermetallics*, 2010, vol. 18, pp. 1385–89.
11. M. Zamanzade and A. Barnoush: *Procedia*, 2014, vol. 3, pp. 2016–23.
12. E. García de León, O. Téllez-Vázquezb, C. Patiño-Carachurec, C. Ángeles-Chávezd, and G. Rosas: *Acta Microscopica*, 2013, vol. 22, pp. 262–68.
13. A.A. Sasikala Devi, U. Schwingenschloegl, and I.S. Roqan: *J. Chem. Phys.*, 2015, vol. 143, p. 224703.
14. A.A. Sasikala Devi and I.S. Roqan: *RSC Adv.*, 2016, vol. 6, pp. 50818–824.
15. A.A. Sasikala Devi and I.S. Roqan: *RSC Adv.*, 2018, vol. 8, pp. 13850–856.
16. J. Wolff, M. Franz, A. Broska, R. Kerl, M. Weinhagen, B. KoÈhler, M. Brauer, F. Faupel, and T. Hehenkamp: *Intermetallics*, 1999, vol. 7, pp. 289–300.
17. J. Bott, H. Yin, and S. Sridhar: *Metall. Mater. Trans. B*, 2014, vol. 45B, pp. 2222–31.
18. S. Ratanaphan, D.L. Olmsted, V.V. Bulatov, E.A. Holm, A.D. Rollett, and G.S. Rohrer: *Acta Mater.*, 2015, vol. 88, pp. 346–54.
19. J. Cheng, J. Luo, and K. Yang: *Comput. Mater. Sci.*, 2018, vol. 155, pp. 92–103.
20. G. Kresse and J. Furthmüller: *Phys. Rev. B*, 1996, vol. 69, p. 54111.
21. P.E. Blöchl: *Phys. Rev. B*, 1994, vol. 50, pp. 17953–17979.
22. J.P. Perdew, K. Burke, and M. Ernzerhof: *Phys. Rev. Lett.*, 1996, vol. 77, p. 3865.
23. A. Janotti and C.G. Van De Walle: *Phys. Rev. B*, 2007, vol. 76, p. 165202.
24. A.A. SasikalaDevi, U. Schwingenschloegl, and I.S. Roqan: *J. Appl. Phys.*, 2014, vol. 116, p. 233906.
25. A.A. Sasikala Devi and I.S. Roqan: *Mater. Res. Exp.*, 2015, vol. 2, p. 12610.
26. Y. Sato and T. Yamamoto: *J. Am. Ceram. Soc.*, 2007, vol. 90 (2), pp. 337–57.
27. W. Körner, P.D. Bristowe, and C. Elsässer: *Phys. Rev. B*, 2011, vol. 84, p. 045305.
28. K. Momma and F. Izumi: *J. App. Crystall.*, 2008, vol. 41, pp. 653–58.
29. P. J. Turner, "XMGRACE, Version 5.1. 19." *Center for Coastal and Land-Margin Research, Oregon Graduate Institute of Science and Technology, Beaverton, OR*, 2.